Programmable Dual-responsive Actuation of Single-hydrogel-based Bilayer Actuators by Photothermal and Skin Layer Effects with Graphene Oxides

*Minghao Li, Jinhye Bae**

M. Li, J. Bae
Materials Science and Engineering Program
University of California San Diego
La Jolla, CA 92093, United States
E-mail: j3bae@ucsd.edu

J. Bae
Department of NanoEngineering
University of California San Diego
La Jolla, CA 92093, United States

J. Bae
Chemical Engineering Program
University of California San Diego
La Jolla, CA 92093, United States

Keywords: stimuli-responsive hydrogels, composite hydrogels, shape morphing, soft actuators, soft robotics

Abstract

Shape morphing of stimuli-responsive composite hydrogels has received considerable attention in different research fields. Although various multilayer structures with dissimilar materials have been studied to achieve shape morphing, combining swellable hydrogel layers with non-swellable layers results in issues with interface adhesion and structural integrity. In this study, single-hydrogel-based bilayer actuators comprising poly(N-isopropylacrylamide) (PNIPAM) matrices and graphene oxide (GO)–PNIPAM hinges are presented. Upon temperature rising, the PNIPAM hydrogel acts as the passive layer due to the formation of dense microstructures near the surface (i.e., the skin layer effect), whereas the GO-PNIPAM hydrogel functions as the active layer, maintaining porous due to structural modification by the presence of GO. Under light exposure, the GO-PNIPAM hinges experience selective heating due to the photothermal

effect of GO. Consequently, the resulting bilayer structures exhibit programmable dual-responsive 3D shape morphing. Additionally, the folding kinetics of these actuators can be adjusted based on the applied stimulus (temperature changes or light), as they are driven by different mechanisms, the skin layer or photothermal effects, respectively. Furthermore, the hinge-based bilayer structures demonstrate walking and steering locomotion by light exposure. This approach could lead to advances in soft robotics, biomimetic systems, and autonomous soft actuators in hydrogel-based systems.

1. Introduction

Shape-morphing polymeric materials have gained long-term interest in different research fields owing to their promising applications in soft actuators, deployable devices, biomimetic systems, and so on.[1-5] Among the various polymeric materials, stimuli-responsive hydrogels offer numerous advantages due to their biocompatibility[6, 7] and volumetric changes by external stimuli such as temperature,[8] pH,[9] ionic strength,[10] and biomolecules.[11] For instance, crosslinked poly(N-isopropylacrylamide) (PNIPAM) is one of the most widely used temperature-responsive hydrogels with a low critical solution temperature (LCST) in a range from 30 to 50 °C depending on end group polarity and molecular weight.[12] PNIPAM hydrogels exhibit a reversible volumetric expansion (i.e., swelling) to contraction (i.e., deswelling) when heated through its LCST.[13] Although immense studies have been reported using the crosslinked PNIPAM hydrogels, their isotropic volume changes and relatively slow swelling kinetics limit their 3D shape transformation and practical applications, respectively.[14, 15] To address these limitations, various photothermal additives have been introduced within the PNIPAM matrix such as carbon nanotubes,[16, 17] iron oxide nanoparticles (IONP),[18, 19] gold nanoparticles (AuNP),[20, 21] and graphene oxide (GO) sheets.[22, 23] Since these photothermal materials convert light to heat, they can trigger the deswelling of the PNIPAM hydrogels by a photothermal-driven internal temperature rise (> LCST) and offer a faster response rate due to

a faster heat conduction.[24, 25] Among these materials, GO offers unique aspects as the oxygen-containing groups and residual C=C double bonds can interact with PNIPAM networks through hydrogen and covalent bonds, respectively.[26, 27] Therefore, incorporating GO affects the internal structure, mechanical property, and responsiveness of PNIPAM hydrogels.[28, 29] For example, PNIPAM hydrogels with uniformly distributed GO demonstrated reversible shape deformation under near-infrared (NIR) light as a microvalve,[30] and an electrical switch.[22] However, such isotropic volume changes are limited to form out-of-plane shape deformation of the composite hydrogel systems.

The 3D shape-morphing of the composite hydrogels can be achieved by the non-uniform volume changes which are introduced by assemblies of dissimilar materials or structural modification.[8, 31] Specifically, GO-PNIPAM composite hydrogels have shown 3D shape transformation via various methods. For example, Ma et al. reported a highly bendable photo-actuator due to the mismatch in the volume change between the active GO-PNIPAM hydrogel layer and the passive polyacrylamide-based layer by a supramolecule glue due to the host-guest interaction.[32] Zhao et al. reported a photo-actuator by local infiltration of GO into PNIPAM hydrogel matrix with a pore size gradient along the thickness direction through hydrothermal reaction.[33] However, the infiltration of GO did not affect the predetermined gradient of pore size. As a result, when exposed to light, the GO-PNIPAM hydrogel folded towards the surface with a larger pore size. Moreover, the degree of folding was determined by the illumination time and was unrelated to the geometry of GO infiltration. This lack of programmability of hydrogel actuators limits the accessible folding angle at equilibrium and the ability to achieve multi-directional folding. Therefore, further study of programmable 3D shape morphing and actuation utilizing a single-hydrogel-based system is necessary.

Skin layer effect of PNIPAM is the formation of a dense outermost PNIPAM network (i.e., skin layer), which is induced due to the deswelling of PNIPAM hydrogels when the temperature abruptly rises above LCST.[34, 35] Such a dense network prevents the outward water

flux, thereby significantly reducing the deswelling ratio of PNIPAM hydrogels.[36] To avoid the formation of skin layers, previous studies have used grafted polymer chains or copolymer synthesis to prevent the formation of skin layers.[37, 38] Recently, we have found that the addition of GO in PNIPAM hydrogels could control the formation of skin layer of PNIPAM upon temperature rising above LCST, thus leading to the different deswelling behaviors of GO-PNIPAM with different GO concentrations.[39] While tunable deformation has been achieved using PNIPAM hydrogel sheets with various GO concentrations, this shape morphing has been limited to simple bending deformation, and the potential of the skin layer effect has not been fully exploited. Therefore, it is necessary to explore the utilization of the skin layer effect to achieve complex shape deformation in the hydrogel actuators.

Here, we demonstrate a single-hydrogel-based bilayer self-folding actuator without assemblies of dissimilar layers or structural modification. Utilizing the tunable deswelling degree of PNIPAM due to the presence of GO, we program a reversible 3D shape morphing of the PNIPAM hydrogel-based system by integrating GO-PNIPAM hinges into a PNIPAM matrix. The hinge-based bilayer structures can undergo self-folding deformations by temperature change and light exposure. Their degree of folding (e.g., folding angle) can be controlled by the hinge width in geometrical design, or the incident angle of light during photothermal-driven actuation. Light exposure results in faster folding kinetics of the hinge-based bilayer structures than temperature change due to absent formation of skin layers and a faster internal temperature rise. The hinge-based bilayer structures with specific structural designs exhibit reversible locomotion such as walking and steering from the selective actuation by light. This study shows the potential promise of single-hydrogel-based systems in the fields of smart soft robotics, programmable actuators, and biomedical devices.

2. Result and Discussion

2.1 Adhesion mechanism of hinge-based bilayer structures. To fabricate the hinge-based bilayer structures, we utilized a layer-by-layer method by free radical polymerization (see Experimental Section for fabrication details and **Figure 1a**). First, GO-PNIPAM pregel solution was injected into the mold and cured (Figure 1a, i and Figure 1b, i). During the partial curing process, NIPAM monomers in GO-PNIPAM pre-gel solution were partially polymerized and crosslinked, which left free radicals on the polymer chains (Figure 1a, ii and Figure 1b, ii). PNIPAM pre-gel solution was subsequently injected into the mold, then polymerized and crosslinked within the GO-PNIPAM networks (Figure 1a, iii and Figure 1b, iii). The polymerization within both layers was completed since most free radicals were consumed (Figure 1a, iv and Figure 1b, iv).

2.2 Stimuli-responsive folding deformation of the hinge-based bilayer structures. We first characterized the temperature-responsive behaviors of the GO-PNIPAM hinge and the PNIPAM matrix by calculating their linear swelling or deswelling ratios (λ_T) where λ_T is defined as D_T/D_0, D_T is the measured diameter at T °C and D_0 is the as-prepared diameter (see Experimental Section for characterization details). The corresponding temperatures for measuring the linear swelling ratio (λ_{23}) and linear deswelling ratio (λ_{38}) were set to 23 °C (room temperature) and 38 °C (> LCST) in the water bath, respectively. At the swelled state, both PNIPAM hydrogel and GO-PNIPAM composite hydrogel have porous structures and absorb water (**Figure 2a**). Therefore, λ_{23} for PNIPAM hydrogels and GO-PNIPAM composite hydrogels are 1.26 ± 0.03 and 1.09 ± 0.03, respectively (Figure S1a, Supporting Information), since the linear swelling ratio of hydrogels decreases with an increase in the crosslinking density.[22] At the deswelled state, λ_{38} of PNIPAM hydrogel and GO-PNIPAM composite hydrogel are 1.09 ± 0.02 and 0.59 ± 0.03 (Figure S1a, Supporting Information), respectively. The deswelling ratio difference at 38 °C between the GO-PNIPAM hinge and the PNIPAM matrix is about 60% which can induce anisotropic volume changes within the hinge-based

bilayer structure by external stimuli (Figure 2b, i). Our group previously reported this phenomenon that the outermost networks of PNIPAM hydrogels collapsed and formed a non-porous layer upon deswelling, which significantly blocks the outward water flux (Figure 2b, ii), whereas the GO-loaded PNIPAM networks could prevent the formation of the dense outermost layer (Figure 2b, iii).[39] Tensile tests were carried out to further study the effect of GO on the mechanical property of GO-PNIPAM composite hydrogels. From the stress-strain curves, the estimated Young's modulus for PNIPAM and GO-PNIPAM are 8 kPa and 40 kPa, respectively (Figure S1b, Supporting Information). Owing to the increasing crosslinking density through the hydrogen bonding between GO and PNIPAM networks,[40] and the rigid nature of GO (Young's modulus of ~400 GPa),[41] GO-PNIPAM composite hydrogel exhibits higher Young's modulus than PNIPAM hydrogel.

To investigate the structural difference between the GO-PNIPAM hinge and the PNIPAM matrix, we characterized the internal microstructure of freeze-dried bilayer structures by scanning electron microscopy (SEM). The distinct microstructures of the GO-PNIPAM hinge and the PNIPAM matrix were continuously conjunct which indicated the formation of interpenetrating PNIPAM networks (Figure 2c). Such interpenetrated networks contribute to the covalent interfacial adhesion between the GO-PNIPAM hinge and the PNIPAM matrix. The pore size difference between the surface of GO-PNIPAM hinge (2.8 ± 2.2 μm in diameter) and the surface of PNIPAM matrix (9.2 ± 2.3 μm in diameter) indicates the effect of GO on the PNIPAM crosslinking density (Figure S2, Supporting Information). The internal pore size becomes smaller in the GO-PNIPAM hinge due to the hydrogen bonding between GO sheets and the PNIPAM networks, thus increasing the crosslinking density within the hinge compared to the PNIPAM matrix.[31, 39] Such continuous networks are maintained at the deswelled state, which indicates a stable adhesion upon deformation (Figure 2d). Moreover, the pore size difference between the surface of GO-PNIPAM hinge (1.1 ± 0.6 μm in diameter) and the

surface of PNIPAM matrix (non-porous) agrees with the formation of the skin layer on the surface of PNIPAM matrix (Figure S3, Supporting Information). We further obtain SEM images of the cross-sectional view of PNIPAM and GO-PNIPAM hydrogels. The dense skin layer of PNIPAM is about 5 μm thick which can significantly suppress outward water diffusion (Figure 2e). The surface of GO-PNIPAM hydrogel maintains porous which allows water to diffuse out from GO-PNIPAM hydrogel, thus resulting in a much smaller λ_{38} (Figure 2f). Interestingly, the surface pore size of GO-PNIPAM at the deswelled state is larger than other pores inside. We believe the cooling of GO-PNIPAM hydrogels in liquid nitrogen during SEM sample preparation causes the swelling of the GO-PNIPAM surface before the structure is frozen. Hence, utilizing such phenomena in this work, PNIPAM served as a "non-shrinkable" passive layer and GO-PNIPAM served as an active layer to generate volume change upon temperature increase above LCST.[42, 43]

Next, we systematically assessed the effect of GO-PNIPAM hinge width w on the degree of folding (i.e., folding angle, θ) of the hinge-based bilayer structures upon heating or light exposure, since the larger volume shrinkage (i.e., smaller deswelling ratio) of the GO-PNIPAM hinge than the PNIPAM matrix induced the out-of-plane deformation toward the hinge direction. A series of bilayer samples were cut into 25 mm x 5 mm with a thickness of 1 mm with prescribed w ranging from 0.5 to 5 mm at the as-prepared state. With an increasing w until 3 mm, θ continuously increased until the bilayer structures reached a completely folded state (θ = 180°) when the temperature was changed from 23 °C to 38 °C abruptly (**Figure 3a**). It depicts the linear dependence of θ on w while fixing all other parameters. Furthermore, the hinge-based bilayer structure exhibited reversible self-folding deformation by repeatedly immersing in the water bath at 23 °C to 38 °C 5 times (Figure S4, Supporting Information). In addition to temperature change, the UV light can induce an internal temperature rise (~ 43 °C) in the GO-PNIPAM hinge due to the photothermal property of GO thus triggering deswelling

of GO-PNIPAM hinges (Figure S5, Supporting Information). By simply varying the hinge width from 0.5 to 5 mm, θ can precisely be controlled from 30° to 180° (Figure 3b). Note that the folding deformation upon light exposure also saturates after reaching θ = 180° when w is above 3 mm. This result exhibits a similar trend to the temperature actuation in Figure 3a.

The hinge-based bilayer structure in Figure 2b shows the width-dependent radius of curvature R of GO-PNIPAM/PNIPAM bilayer bending, which can be analytically predicted by the modified Timoshenko bimorph beam theory[44, 45]:

$$R = \frac{(h_G+h_P)(8(1+m)^2+(1+mn)(m^2+\frac{1}{mn})}{6\varepsilon(1+m)^2}, \quad (1)$$

Where $m = h_P/h_G$ is the thickness ratio of the PNIPAM matrix (h_P) to the GO-PNIPAM hinge (h_G), $n = E_P/E_G$ is the ratio of elastic modulus of the PNIPAM matrix (E_P) to the GO-PNIPAM hinge (E_G) which is obtained from Figure 2a, and ε is the difference in actuation strain between the two layers (Table S1). Here the actuation strain is calculated by the mismatch of the linear deswelling ratio at 38 °C between the PNIPAM matrix ($\lambda_{38,P}$) and the GO-PNIPAM hinge ($\lambda_{38,G}$):

$$\varepsilon = \varepsilon_G - \varepsilon_P = (1-\lambda_{38,G}) - (1-\lambda_{38,P}). \quad (2)$$

The theoretical folding angle, θ is calculated by the radius of the curvature as $\theta = \frac{180w}{\pi R}$ (3). The experimental data is in good agreement with the theoretical calculations by a linear relationship (Figure 3a and b). This result supports that the degree of folding of the hinge-based bilayer structure can be systematically programmed by varying the widths of GO-PNIPAM hinges.

2.3 Self-folding kinetics of the hinge-based bilayer structures by temperature change and light exposure. To characterize the self-folding kinetics under heating and light exposure, five hinge-based bilayer structures with a hinge width of 5 mm were prepared. Bilayer structures reached a completely folded state after immersing in water at 38 °C for 1 hour (**Figure 4a**,

Supplementary Movie 1). However, photothermal-driven actuation induced the complete folding of bilayer structures in 3 minutes (Figure 4b, Supplementary Movie 2). The self-folding kinetics of bilayer structures is presumably associated with multiple phenomena, also affected by the intrinsic properties of PNIPAM networks and GO. Here, we hypothesize that the difference in self-folding kinetics under heating and light exposure may be due to the following reasons. First, photothermal-driven actuation by GO can readily lead to a higher temperature than 38 °C in GO-PNPAM owing to the more effective heat conduction through GO and less heat dissipation to the environment (Figure S5b).[24] Second, upon abrupt heating, the PNIPAM matrix forms a dense non-porous outermost layer to prevent the outward water flux which results in a higher deswelling ratio (Figure S1a).[39] The formation of a non-porous layer at the interfaces between the PNIPAM matrix and the GO-PNIPAM hinge can hinder the effective water expel from the hinge while deswelling by abruptly transferring from room temperature (23°C) water to hot water at 38 °C. On the other hand, light exposure selectively leads to the deswelling of the GO-PNIPAM hinge therefore water can diffuse out from the hinge to the matrix more effectively. Third, the temperature-triggered folding can require more bending energy through the hinge-matrix bilayer since the Young's modulus of deswelled PNIPAM is typically one order of magnitude greater than swelled PNIPAM.[46] In contrast, the PNIPAM matrix remains the swelled state upon photothermal-driven actuation thus this folding deformation is energetically less expensive than temperature actuation when the hinge undergoes a similar degree of deswelling.[47] Therefore, we anticipate that further miniaturization of the bilayer can be the most effective approach to improve the folding kinetics of hydrogel-based actuators, also changing the composition of the matrix material in order to reduce the modulus or increase porosity can be an additional approach. Moreover, we compare our GO-PNIPAM/PNIPAM bilayer actuator to PNIPAM/hydrogel bilayer actuators and PNIPAM/non-hydrogel bilayer actuators (Table S2). Our GO-PNIPAM/PNIPAM bilayer actuator has outstanding actuation amplitude and adequate actuation kinetics (0.06 s^{-1})

compared with PNIPAM/hydrogel bilayer actuators and PNIPAM/non-hydrogel bilayer actuators. An outstanding actuation amplitude is owing to the relatively large actuation strain and low Young's modulus of both GO-PNIPAM and PNIPAM layers compared to PNIPAM/hydrogel bilayer actuators and PNIPAM/non-hydrogel bilayer actuators, respectively. While our GO-PNIPAM/PNIPAM bilayer actuator exhibits a slower actuation kinetic than liquid crystal systems (0.1 – 10 s^{-1}),[48-50] it is worth noting that liquid crystal systems typically require higher phase transition temperatures (55 - 150 °C),[51] which are significantly higher than the LCST of PNIPAM (32 °C). Therefore, they are subject to energy transfer efficiency and operation temperature which have greatly limited their biological applications.[52-54]

2.4 Programmable folding behaviors by self-shadowing effect. Next, we studied how θ is related to the direction of light irradiation by varying the angle of the light source relative to the hinge-based bilayer structures. As the light was coming from the top of the hinge (90° tilted to the ground), θ was not able to reach 180° but oscillated about 120° (**Figure 5a**, Supplementary Movie 3). During the light exposure, the GO-PNIPAM hinge was quickly shrunk then the entire bilayer began to fold. However, when θ exceeded 90°, the near end of the hinge toward the light source started to block the light to the far end of the hinge, which is the so-called self-shadowing effect.[55, 56] The blocked area underwent continuous cooling until the temperature of the far end of the hinge decreased below the LCST, leading to reswelling until the blocked area was re-exposed to light. As the light source was tilted 45° toward the ground, the entire hinge could be exposed by the UV light. Thus, the bilayer structure could undergo complete folding. To test the reversibility of self-folding deformation of hinge-based bilayer structures, five bilayer structures with a hinge width of 5 mm were deformed through the light on-and-off cycles in different directions. The samples exposed to 45° UV light could reach complete folding at least until 5 cycles as samples exposed to 90° UV lights oscillated about 125° ± 5.7°

(Figure 5b). Therefore, changing the incident angle of light provides a simple means to control θ using the same geometry of hinge-based bilayer structures with reproducible results.

2.5 Biomimetic demonstrations of the hydrogel actuators. By utilizing faster and controllable actuation of the GO-PNIPAM/PNIPAM bilayer structures by UV light, programmable and smart soft actuators were further designed and fabricated for biomimetic demonstrations. We first demonstrated the selective light actuation in a hinge-based bilayer structure which was prepared with a size of 25 mm x 5 mm with a thickness of 1mm at the as-prepared state. Two hinges (i and ii) which had lateral widths of 5 mm, were located on opposite surfaces (**Figure 6a**). After exposing 365 nm UV (intensity 1.1 W cm^{-2}) for 30 seconds, each hinge can be selectively actuated by UV light and resulting in self-folding deformation. Hinge i and ii showed θ of 94° and 105°, respectively (Figure 6b). Folding angle result of hinge i agrees with the folding kinetics of 30-second exposure in Figure 4b. However, hinge ii obtained a larger θ which was presumably due to the increasing intensity of UV as hinge ii bent toward the light source under the exposure. The hinge-based bilayer structures exhibited distinct folding directions toward the hinge position. With this advantage, we can program complex folding-based 3D shapes and motions with selective actuation.

Utilizing the selective actuation of hinges in the bilayer structure, we designed a hydrogel walking actuator with two GO-PNIPAM hinges (i and ii) located on the opposite surfaces of the PNIPAM matrix inspired by an inchworm movement (Figure 6c).[57] When the hinge i was exposed to UV light, the sample folded upward, resulting in only two ends of the bilayer supporting the walking actuator. When the light was turned off, the walking actuator recovered back to its original state by flattening its body. Note that each light actuation process is composed of 30-second UV on (deformation) and 30-second UV off (recovery). The asymmetric design of the walking actuator determined the direction of movement by a friction difference between the hinge ii-side end and the opposite end. During the light actuation process,

the friction f_a between the tip of the opposite end with no hinge and the glass substrate was much smaller than the friction f_b between the PNIPAM surface underneath hinge ii and the glass substrate, due to the larger contact area of a bent end with hinge ii (Figure 6d).[58]This process was repeatable and the hydrogel walking actuator could continuously move in a single direction. The actual walking process of the hydrogel actuator was achieved when the light was irradiating directly from the top of the hinge i (Figure 6e, Supplementary Movie 4). The walking actuator moved forward 10 mm in two light on-off cycles. The average speed of movement is 5 mm per minute. Moreover, this walking process could also be adjusted by the direction of light irradiation. When the direction of light was tilted 45° toward the ground, the light was not able to cover the entire hinge i as the further side of the hinge i toward light was not illuminating (Figure 6f). It resulted in a smaller θ (~ 40°) compared with light irradiating from the top of the hinge i (θ ~ 100°). Thus, the walking distance for the same design of the actuator was reduced to 5 mm in two cycles compared to 90° tilted UV light irradiation.

Next, we designed a hydrogel steering actuator with two legs and three hinges (i, ii and iii) (**Figure 7a**) to achieve more complex locomotion. Similar to the hydrogel walking actuator, hinge i was exposed by UV light for 30 s and recovered after turning off UV for 30 seconds (Figure 7b). When UV was applied to the exposure area, the leg with hinge i was deformed, generating friction f between the bottom surface of the leg with hinge i and the glass substrate. However, f was not in the central axis of the actuator due to the asymmetric deformation of the actuator. Therefore, the steering motion resulted from the mismatch between the friction direction and central axis,[59] thus generating torque to the actuator. Figure 7c shows the continuous steering motion by exposing UV to hinge i: From repetition 0 (initial state) to repetition 3 (third UV on-and-off cycle), the hydrogel steering actuator turned about 45° clockwise, indicating a continuous movement (Supplementary Movie 5). These results

demonstrate the smart locomotion actuator can be designed and easily controlled by selective light irradiation.

3. Conclusion

In summary, we have reported a single-hydrogel-based bilayer actuator with self-folding and locomotion by fabricating hinge-based GO-PNIPAM/PNIPAM bilayer structures. Herein the GO serves as both a photothermal additive and a physical crosslinker to change the responsiveness and microstructure of PNIPAM hydrogels, respectively. Due to the skin layer effect difference between the GO-PNIPAM hinge and the PNIPAM matrix, the hinge-based bilayer structures created anisotropic volume changes under temperature change and light exposure. When the temperature raised above the LCST of the PNIPAM, the GO-PNIPAM hinges shrunk much more than the PNIPAM matrix, which induced reversible out-of-plane deformation (i.e., self-folding) of hinge-based bilayer structures. Due to the photothermal effect of GO, UV light can also trigger the internal temperature increase of patterned GO-PNIPAM composite hydrogels. The degree of folding of the bilayer structures could be controlled by varying hinge widths under temperature change and light exposure, and the angle of incident light while photothermal-driven actuation. The type of stimuli could significantly change the kinetics of shape deformation, where light exposure could accelerate folding kinetics 20 times faster than temperature change due to a faster water diffusion rate. We have also demonstrated that the folding direction was determined by the position of the hinge. The selective light exposure allows the spatial and temporal control of self-folding thus programmable locomotion, such as walking and steering motion. We anticipate the single-hydrogel-based stimuli-responsive actuators with programmable reversible self-folding behaviors and locomotion, can provide inspiration for potential applications in stimuli-responsive actuators, biomedical devices, and biomimetic systems.

Experimental section

Materials: N-isopropylacrylamide (NIPAM, stabilized with 4-methoxyphenol) was purchased from Tokyo Chemical Industry (TCI) America. Aqueous graphene oxide (GO, 6.2 mg mL^{-1}, flake size: 0.5-5 μm) was obtained from Graphene Supermarket (Calverton, NY, USA). N,N'-methylenebisacrylamide (BIS), N,N,N',N'-tetramethylethylenediamine (TEMED), and ammonium persulfate (APS) were all obtained from Sigma-Aldrich (St Louis, MO, USA). All chemicals were used as received without further purification. Water used throughout experiments was purified by a Millipore purification system (MilliporeSigma, MA, USA).

Preparation of pre-gel solutions. Pre-gel solutions (8.5 mL) were prepared by mixing NIPAM, BIS, aqueous GO, and water with a vortex mixer (Dlab Mx-S) at room temperature until all solids were dissolved. GO-NIPAM pre-gel solution contained GO (21.25 mg, 3.43 mL) as photothermal additives, NIPAM (839 mg, 872 mM) as a monomer and BIS (11 mg, 9 mM) as a chemical crosslinker. NIPAM pre-gel solution was prepared with identical chemical composition to GO-NIPAM pre-gel solution except for the GO additives. For each pre-gel solution, a continuous nitrogen flow was pumped into the batch container for 4 minutes to remove oxygen which would hinder free radical polymerization.[60] Then, the solution container was sealed and transferred into a larger container. A continuous nitrogen flow was pumped into the larger container for 30 seconds to remove oxygen again. Next, both containers were transferred into a sealed glove box fulfilled with nitrogen. The pre-gel solution was left standing for 30 minutes before polymerization.

Preparation of hinge-based bilayer structures. The preparation of hinge-based bilayer structures is schematically illustrated in Figure 1a. To prepare hinge-based GO-PNIPAM/PNIPAM bilayer structures, firstly 15 μL TEMED as an accelerator and 50 μL aqueous APS (10 wt%) as an initiator were loaded into GO-NIPAM pre-gel solution to initiate

free radical polymerization. The resulting pre-gel solution was then injected into a mold which was made with two clean glass slides (75 mm × 25 mm) separated by Kapton film spacers for 0.3 mm. GO-PNIPAM composite hydrogel was partially polymerized at 23 °C for 15 minutes. At this stage, the batch solution was solidified but the polymerization was still ongoing. Next, the top cover slide was removed, 0.3 mm spacers were replaced by 1 mm Kapton film spacers, and then the cover slide was re-applied. Following that 15 μL TEMED and 50 μL aqueous APS (10 wt%) were loaded into NIPAM pre-gel solution to initiate free radical polymerization. The resulting NIPAM pre-gel solution was injected into the mold to fully immerse GO-PNIPAM composite hydrogel. The polymerization was carried in the glove box fulfilled with nitrogen for 3.5 hours. After polymerization, the glass slides and spacers were removed, then the hinge-based bilayer structures were cut to the designated shape and immersed in water for 72 hours to swell. For the first three-hour immersion, water was replaced every hour to remove all unreacted chemicals. Single GO-PNIPAM and PNIPAM hydrogel sheets were prepared separately under the same conditions for characterizing their properties, respectively.

Swelling and deswelling behaviors of single GO-PNIPAM and PNIPAM sheets. To characterize the swelling/deswelling behaviors of single PNIPAM and GO-PNIPAM sheets, five samples of each composition were biopsy-punched into thin disks with 5 mm diameter and, 0.3 mm and 0.7 mm thickness in the as-prepared state, respectively. The samples were kept in the water at 23 °C for 72 hours to swell. Subsequently, samples were transferred into the water at 38 °C for 1 hour to deswell since the initial deswelling at 1 hour was more predominant in our previous work.[34] The sizes of samples at different states were recorded by an optical microscope (Keyence VHX).

Characterization of the mechanical properties of GO-PNIPAM and PNIPAM sheets. The mechanical properties are characterized by the tensile test. PNIPAM and GO-PNIPAM composite hydrogels (thickness of 1 mm at as-prepared state) were fully swelled in water at

room temperature (23 °C) for 72 hours and cut to 25 mm × 8 mm by punch cutter, respectively. Then the hydrogel sheet was loaded to a tensile instrument (Instron, Bluehill, MA, USA) with a 100 N load cell. The strech rate was set to 10 mm per minute. The tensile stress was defined as the force applied to the deformed hydrogel divided by the real-time characteristic cross-sectional area of the deformed hydrogel. The Young's modulus (E) of the hydrogel at a certain tensile strain was calculated by the slope of the stress−strain curve at the breaking point.

Self-folding and locomotion of hinge-based GO-PNIPAM/PNIPAM bilayer structures. Hinge-based GO-PNIPAM/PNIPAM bilayer structures with different widths of GO-PNIPAM hinges were cut as length, width, and thickness were 25, 5, and 1 mm in the as-prepared state, respectively. To investigate the folding deformation by temperature change, fully swelled hydrogel bilayer structures were immersed in 38 °C water for 1 hour. To investigate the folding deformation and locomotion under light exposure, an ultraviolet (UV) system (Omnicure S2000, wavelength: 365 nm, Lumen Dynamics, ON, Canada) with a tunable output power (0-40 W) was used as the light source throughout the experiments. The exposed light toward the hinge was at 45 ° or 90° tilted to the ground. The UV intensity was fixed at 1.1 W cm^{-2}. The light spot had a diameter of 2 cm which was greater than the entire hinge size to ensure the coverage of the GO-PNIPAM hydrogel hinge. Single-hydrogel-based bilayer actuators were immersed in 23 °C water through light exposure. The spacing between the light source and sample was fixed at 10 cm. The folding angle θ was measured by ImageJ software.

Microstructure characterization of hinge-based GO-PNIPAM/PNIPAM bilayer structures. The microstructures of freeze-dried hinge-based bilayer structures were characterized by scanning electron microscopy (SEM) (FEI Quanta FEG 250). To prepare freeze-dried swelled samples, the bilayer structures were first immersed in water at 23 °C for at least 72 hours to allow them to reach the fully swelled state. To prepare freeze-dried deswelled samples, the bilayer structures were immersed in water at 38 °C for at least 1 hour to

allow them to reach the fully deswelled state. Next, these samples were rapidly frozen in liquid nitrogen for 10 minutes. The frozen samples were dried by a freeze dryer (Labconco FreeZone) at - 80 °C for 72 hours. The freeze-dried samples were coated with iridium before SEM imaging to prevent the charging of specimens.

Statistical Analysis. All data were expressed as mean ± standard deviation. A minimum of five tests were performed for swelling ratio measurement, tensile test, reversibility test and folding angle measurement to ensure that reported results were significant.

Supporting Information

Supporting Information is available from the Wiley Online Library or from the author.

Acknowledgements

This work was supported by the National Science Foundation (CBET-2224740), with additional support from the National Science Foundation through the UC San Diego Materials Research Science and Engineering Center (UCSD MRSEC), grant number DMR-2011924.

Received: ((will be filled in by the editorial staff))
Revised: ((will be filled in by the editorial staff))
Published online: ((will be filled in by the editorial staff))

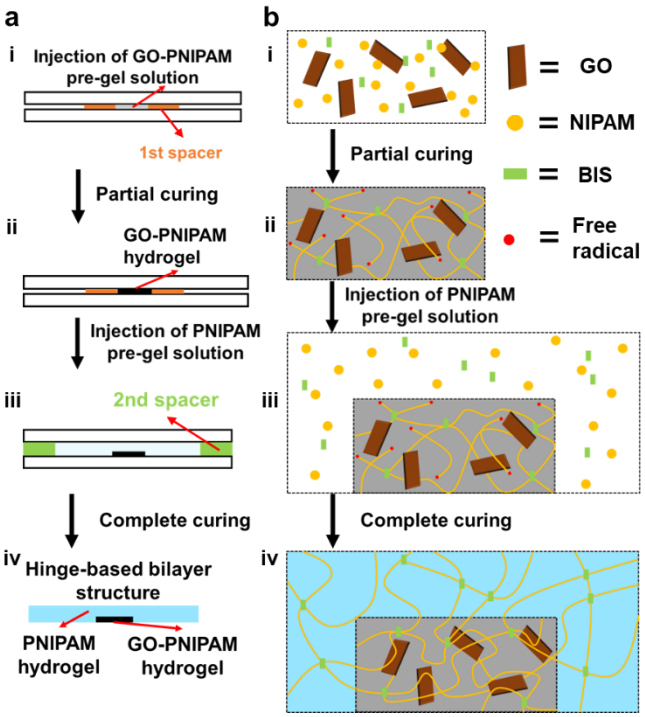

Figure 1. (a) The schematic illustrations of a layer-by-layer fabrication method of a hinge-based bilayer structure through free radical polymerization. (b) The schematic illustrations of the adhesion mechanism of the hinge-based bilayer structure correspond to each step of the fabrication method in (a). (a, i and b, i) Injection of GO-PNIPAM pregel solution, (a, ii and b, ii) partial curing of GO-PNIPAM hinge, (a, iii and b, iii) injection of PNIPAM pregel solution, (a, iv and b, iv) complete curing of both layers.

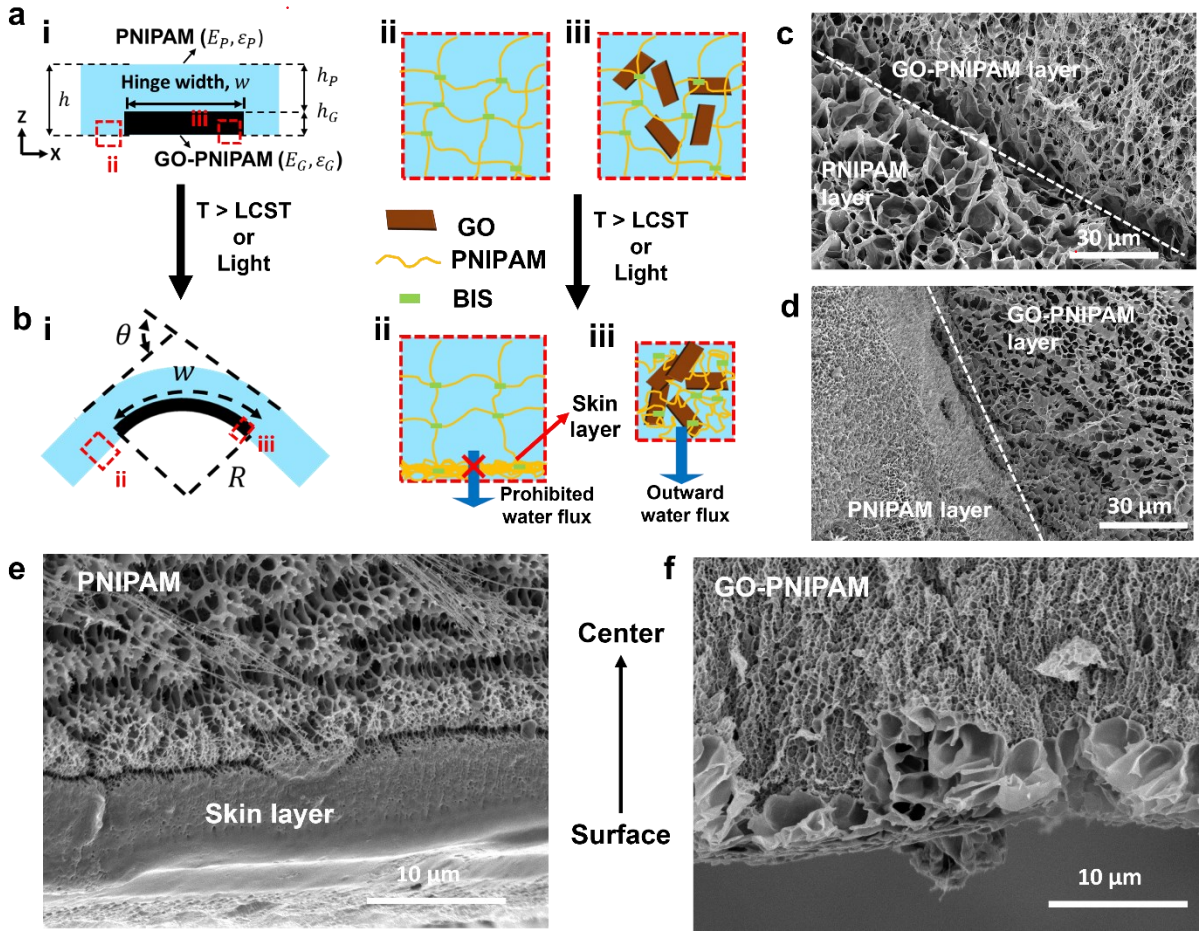

Figure 2. Schematic illustration of the self-folding mechanism of the hinge-based bilayer actuators with hinge width w by temperature change and light exposure at (a, i) swelled and (b, i) deswelled states. Young's modulus, actuation strain, thickness of the GO-PNIPAM hinge and the PNIPAM matrix are represented by E_G, ε_G, h_G and E_P, ε_P, h_P, respectively. Schematic illustration of the internal structures of (a, ii and b, ii) PNIPAM layer and (a, iii and b, iii) GO-PNIPAM layer. SEM images of the top view of the interface between freeze-dried GO-PNIPAM hinge and PNIPAM matrix at (c) swelled and (d) deswelled states. SEM images of the cross-sectional view of freeze-dried (e) PNIPAM layer and (f) GO-PNIPAM layer at deswelled state.

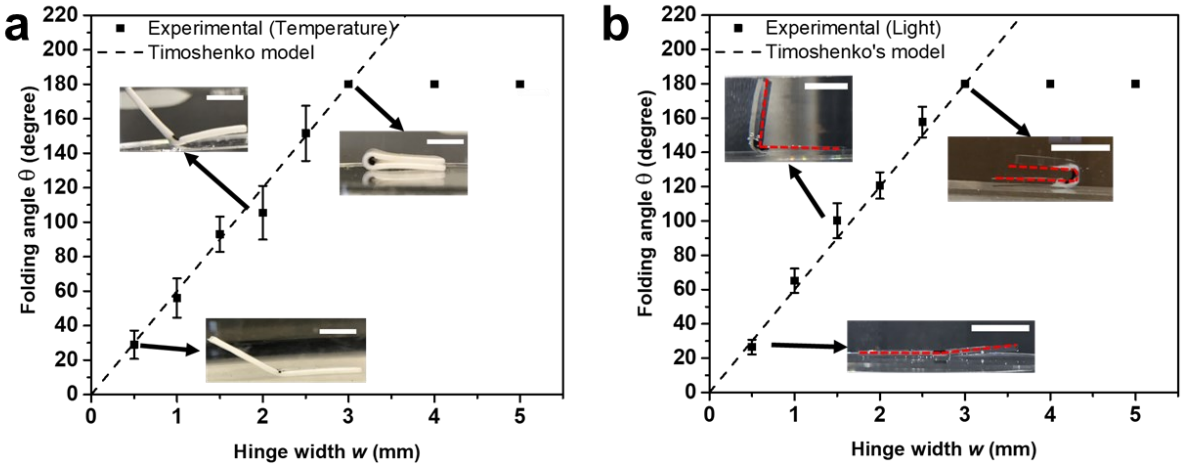

Figure 3. Sample deforms to a folding angle θ due to anisotropic deswelling between the GO-PNIPAM hinge and the PNIPAM matrix in response to (a) temperature and (b) light actuation. Measured (dots) and predicted (dash line) θ are as a function of the hinge width. The predicted result corresponds to the modified Timoshenko's bimorph model. The error bars capture the first standard deviation with a minimum of 5 samples of each hinge width with all other variables held in constant. Inserted images are folded samples with different hinge widths. The red dotted lines in the inset images were used to indicate the contour of the bilayer structure. Scale bar is 5 mm.

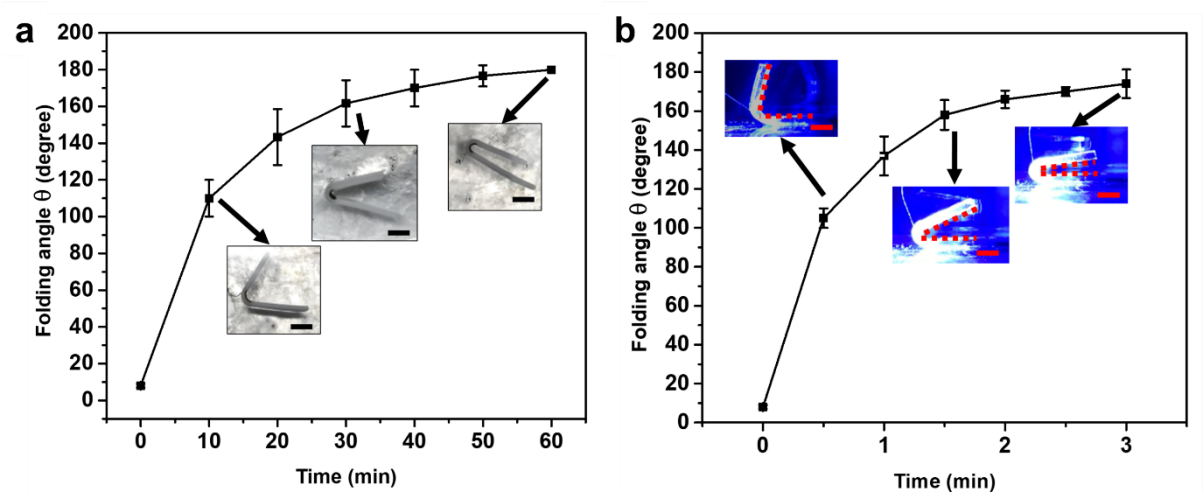

Figure 4. Kinetics of bilayer structure by (a) temperature and (b) light actuation. The hinge size is 5 mm, 5 mm, and 0.3 mm in width, length, and thickness, respectively. Matrix size is 25 mm, 5mm, and 1 mm in width, length, and thickness, respectively. Both sizes are measured at the as-prepared state. For temperature actuation, the hydrogel was immersed in water at 38 °C. For light actuation, 1.1 W cm^{-2} 365nm UV was used. Scale bar is 5 mm.

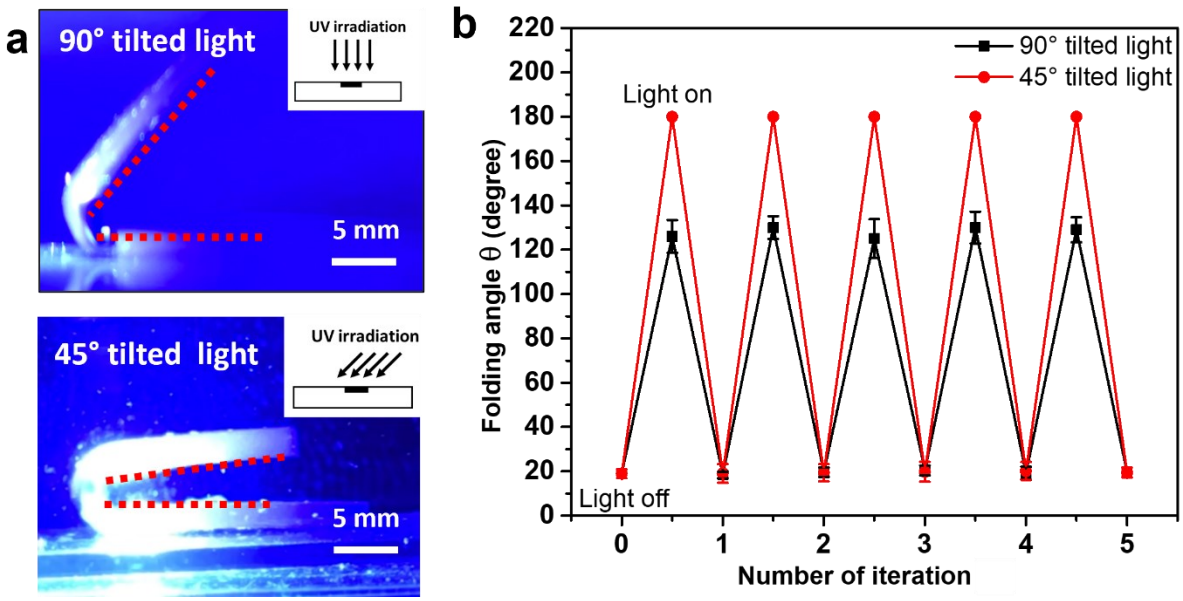

Figure 5. (a) Bilayer structures folded after exposure of 90° and 45° tilted light. (b) Reversibility of folded bilayer structure by different light directions. The hinge width was 5 mm. The intensity of UV light was kept as 1.1 W cm^{-2} throughout the entire experiment. The red dotted lines were used to indicate the contour of the bilayer structure. The inserted images are schematics of light direction.

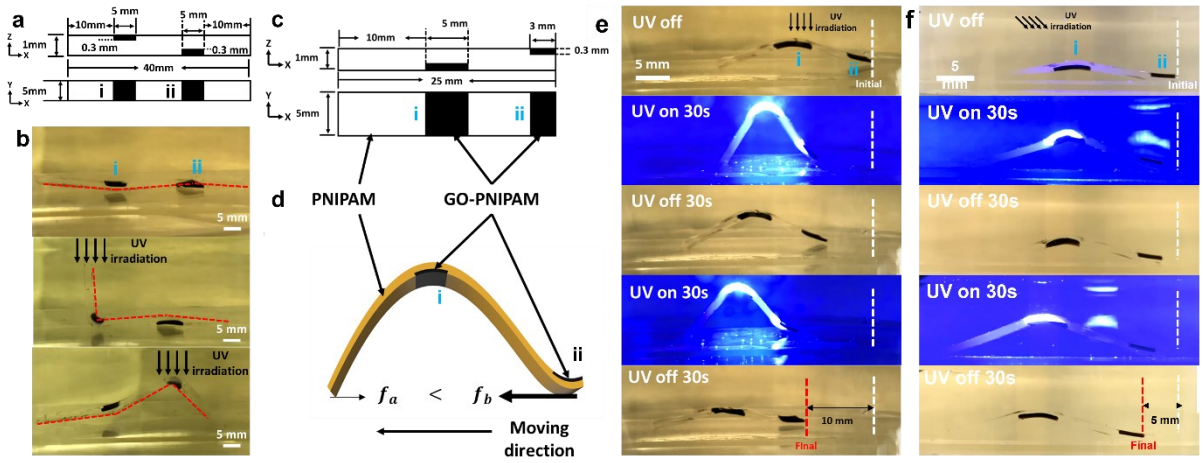

Figure 6. Biomimetic soft walking actuator. (a) Selective actuation of hinges in the hinge-based bilayer structure with two hinges (i and ii) located on the opposite surface of bilayer structure; (b) selective actuation of each hinge which leads to opposite folding direction. (c) Design of soft walking actuator; (d) the schematic diagram of the soft walking actuator; the movement process of the soft walking actuator under (e) 90° and (f) 45 ° tilted UV light irradiation.

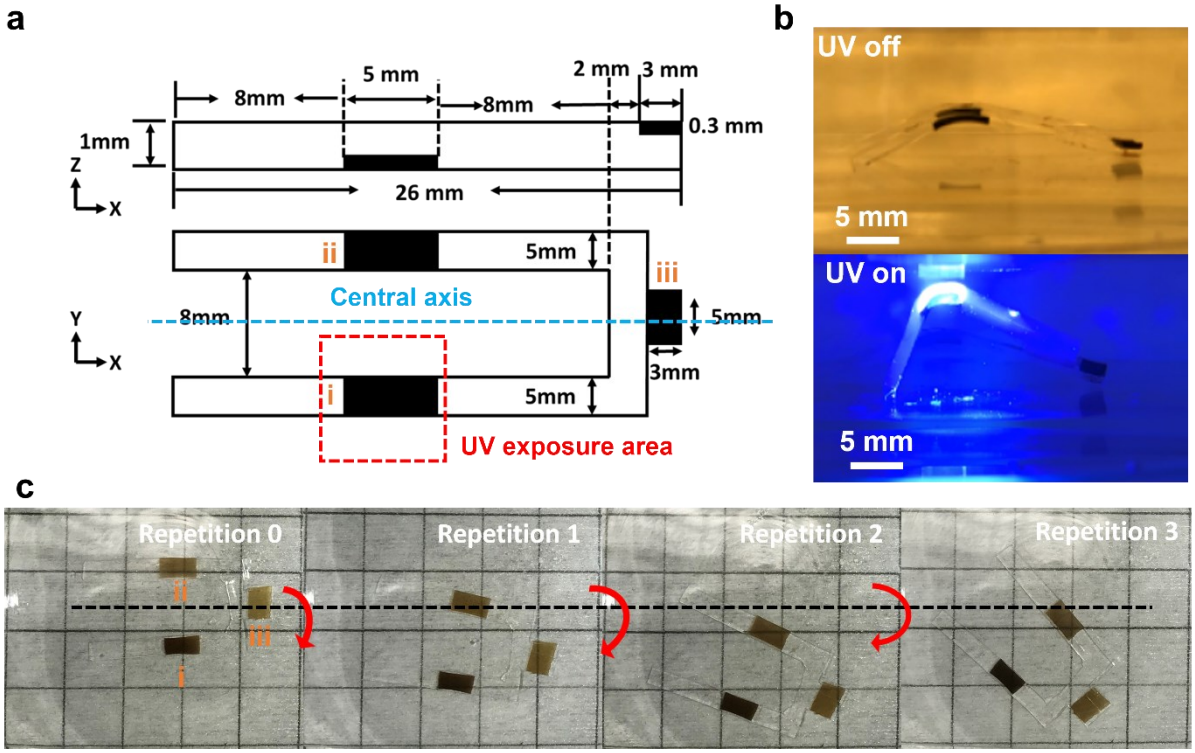

Figure 7. Biomimetic soft steering actuator. (a) design of soft steering actuator with three hinges (i, ii and iii) and selective actuating hinge i by UV exposure at 1.1 W/cm^2; (b) optical images of the side view of steering actuator when UV source was turned on and off; (c) the steering process of the soft actuator under interval UV light on a grid background. Each grid has a length of 10 mm. The red dotted lines in (a) were used to indicate the contour of the hinge-based bilayer structure. The black dotted line in (c) indicates the original position of geometric symmetry through repetition 0 to 3.

References

[1] R. Kempaiah, Z. Nie, *J. Mater. Chem. B* **2014**, 2, 2357.
[2] L. Ionov, *Langmuir* **2015**, 31, 5015.
[3] K. Sano, Y. Ishida, T. Aida, *Angew. Chem., Int. Ed. Engl.* **2018**, 57, 2532.
[4] J. Liu, O. Erol, A. Pantula, W. Liu, Z. Jiang, K. Kobayashi, D. Chatterjee, N. Hibino, L. H. Romer, S. H. Kang, T. D. Nguyen, D. H. Gracias, *ACS Appl. Mater. Interfaces* **2019**, 11, 8492.
[5] S. Nam, E. Pei, *Prog. Addit. Manuf.* **2019**, 4, 167.
[6] P. Abdollahiyan, B. Baradaran, M. de la Guardia, F. Oroojalian, A. Mokhtarzadeh, *J Control Release.* **2020**, 328, 514.
[7] S. Chatterjee, P. C.-l. Hui, *Polymers* **2021**, 13, 2086.
[8] J. Zhao, J. Bae, *Adv. Funct. Mater.* **2022**, 2200157.
[9] A. Richter, G. Paschew, S. Klatt, J. Lienig, K.-F. Arndt, H.-J. P. Adler, *Sensors* **2008**, 8, 561.
[10] J. C. Athas, C. P. Nguyen, S. Kummar, S. R. Raghavan, *Soft Matter* **2018**, 14, 2735.
[11] R. V. Ulijn, N. Bibi, V. Jayawarna, P. D. Thornton, S. J. Todd, R. J. Mart, A. M. Smith, J. E. Gough, *Mater. Today* **2007**, 10, 40.
[12] S. Furyk, Y. Zhang, D. Ortiz-Acosta, P. S. Cremer, D. E. Bergbreiter, *J. Polym. Sci., Part A-1: Polym. Chem.* **2006**, 44, 1492.
[13] S. J. Jeon, A. W. Hauser, R. C. Hayward, *Acc Chem Res* **2017**, 50, 161.
[14] J. Wu, Y. Lin, J. Sun, *J. Mater. Chem.* **2012**, 22, 17449.
[15] A. W. Hauser, A. A. Evans, J. H. Na, R. C. Hayward, *Angew. Chem., Int. Ed. Engl.* **2015**, 54, 5434.
[16] S. Lu, B. Panchapakesan, *Nanotechnology* **2007**, 18, 305502.
[17] X. Zhang, C. L. Pint, M. H. Lee, B. E. Schubert, A. Jamshidi, K. Takei, H. Ko, A. Gillies, R. Bardhan, J. J. Urban, M. Wu, R. Fearing, A. Javey, *Nano Lett.* **2011**, 11, 3239.
[18] R. Hernandez, C. Mijangos, *Macromol. Rapid Commun.* **2009**, 30, 176.
[19] J. C. Breger, C. Yoon, R. Xiao, H. R. Kwag, M. O. Wang, J. P. Fisher, T. D. Nguyen, D. H. Gracias, *ACS Appl. Mater. Interfaces* **2015**, 7, 3398.
[20] Y. Zhou, A. W. Hauser, N. P. Bende, M. G. Kuzyk, R. C. Hayward, *Adv. Funct. Mater.* **2016**, 26, 5447.
[21] H. Kim, J. H. Kang, Y. Zhou, A. S. Kuenstler, Y. Kim, C. Chen, T. Emrick, R. C. Hayward, *Advanced Materials* **2019**, 31, 1900932.
[22] K. Shi, Z. Liu, Y. Y. Wei, W. Wang, X. J. Ju, R. Xie, L. Y. Chu, *ACS Appl. Mater. Interfaces* **2015**, 7, 27289.
[23] M. Li, J. Mei, J. Friend, J. Bae, *Small* **2022**, 2204288.
[24] C.-W. Lo, D. Zhu, H. Jiang, *Soft Matter* **2011**, 7, 5604.
[25] X. Peng, T. Liu, C. Jiao, Y. Wu, N. Chen, H. Wang, *J. Mater. Chem. B* **2017**, 5, 7997.
[26] J. Qi, W. Lv, G. Zhang, F. Zhang, X. Fan, *Polym. Chem.* **2012**, 3, 621.
[27] A. GhavamiNejad, S. Hashmi, H. I. Joh, S. Lee, Y. S. Lee, M. Vatankhah-Varnoosfaderani, F. J. Stadler, *Phys Chem Chem Phys* **2014**, 16, 8675.
[28] M. A. Haq, Y. Su, D. Wang, *Mater Sci Eng C Mater Biol Appl* **2017**, 70, 842.
[29] O. Czakkel, B. Berke, K. László, *Eur. Polym. J.* **2019**, 116, 106.
[30] C.-H. Zhu, Y. Lu, J. Peng, J.-F. Chen, S.-H. Yu, *Adv. Funct. Mater.* **2012**, 22, 4017.
[31] L. Tang, L. Wang, X. Yang, Y. Feng, Y. Li, W. Feng, *Prog. Mater. Sci.* **2021**, 115.
[32] C. Ma, W. Lu, X. Yang, J. He, X. Le, L. Wang, J. Zhang, M. J. Serpe, Y. Huang, T. Chen, *Adv. Funct. Mater.* **2018**, 28.
[33] Q. Zhao, Y. Liang, L. Ren, Z. Yu, Z. Zhang, L. Ren, *Nano Energy* **2018**, 51, 621.
[34] Y. Kaneko, R. Yoshida, K. Sakai, Y. Sakurai, T. Okano, *J. Membr. Sci.* **1995**, 101, 13.
[35] E. S. Gil, S. M. Hudson, *Biomacromolecules* **2007**, 8, 258.

[36] D. M. Solis, A. Czekanski, *Soft Matter* **2022**, 18, 3422.
[37] Y. Kaneko, S. Nakamura, K. Sakai, T. Aoyagi, A. Kikuchi, Y. Sakurai, T. Okano, *Macromolecules* **1998**, 31, 6099.
[38] Y. Kaneko, K. Sakai, A. Kikuchi, Y. Sakurai, T. Okano, presented at *Macromol. Symp.* **1996**.
[39] M. Li, J. Bae, *Polym. Chem.* **2020**, 11, 2332.
[40] Z. Zhu, Y. Li, H. Xu, X. Peng, Y.-N. Chen, C. Shang, Q. Zhang, J. Liu, H. Wang, *ACS Appl. Mater. Interfaces* **2016**, 8, 15637.
[41] L. Liu, J. Zhang, J. Zhao, F. Liu, *Nanoscale* **2012**, 4, 5910.
[42] E. Zhang, T. Wang, W. Hong, W. Sun, X. Liu, Z. Tong, *J. Mater. Chem. A* **2014**, 2.
[43] Z. Tang, Z. Gao, S. Jia, F. Wang, Y. Wang, *Adv. Sci.* **2017**, 4, 1600437.
[44] S. Timoshenko, *Josa* **1925**, 11, 233.
[45] H. W. Huang, M. S. Sakar, A. J. Petruska, S. Pane, B. J. Nelson, *Nat. Commun.* **2016**, 7, 12263.
[46] J. Zhao, H. Kazemi, H. A. Kim, J. Bae, *Soft Matter* **2022**, 18, 8771.
[47] J. Bae, T. Ouchi, R. C. Hayward, *ACS Appl. Mater. Interfaces* **2015**, 7, 14734.
[48] H. Shahsavan, A. Aghakhani, H. Zeng, Y. Guo, Z. S. Davidson, A. Priimagi, M. Sitti, *Proc Natl Acad Sci U S A* **2020**, DOI: 10.1073/pnas.1917952117.
[49] A. S. Kuenstler, H. Kim, R. C. Hayward, *Adv Mater* **2019**, 31, 1901216.
[50] T. J. White, N. V. Tabiryan, S. V. Serak, U. A. Hrozhyk, V. P. Tondiglia, H. Koerner, R. A. Vaia, T. J. Bunning, *Soft Matter* **2008**, 4, 1796.
[51] L. Dong, Y. Zhao, *Mater. Chem. Front.* **2018**, 2, 1932.
[52] H. E. Fowler, P. Rothemund, C. Keplinger, T. J. White, *Adv Mater* **2021**, 33, 2103806.
[53] L. Qin, X. Liu, Y. Yu, *Adv. Opt. Mater.* **2021**, 9, 2001743.
[54] Q. He, Z. Wang, Y. Wang, Z. Song, S. Cai, *ACS Appl. Mater. Interfaces* **2020**, 12, 35464.
[55] Y. Zhao, C. Xuan, X. Qian, Y. Alsaid, M. Hua, L. Jin, X. He, *Sci. Rob.* **2019**, 4, eaax7112.
[56] J. Qin, K. Chu, Y. Huang, X. Zhu, J. Hofkens, G. He, I. P. Parkin, F. Lai, T. Liu, *Energy Environ. Sci.* **2021**, 14, 3931.
[57] W. Wang, J.-Y. Lee, H. Rodrigue, S.-H. Song, W.-S. Chu, S.-H. Ahn, *Bioinspir. Biomim.* **2014**, 9, 046006.
[58] Y. Dong, J. Wang, X. Guo, S. Yang, M. O. Ozen, P. Chen, X. Liu, W. Du, F. Xiao, U. Demirci, B. F. Liu, *Nat. Commun.* **2019**, 10, 4087.
[59] Y. Yang, Y. Shen, *Adv. Opt. Mater.* **2021**, 9, 2100035.
[60] P. Chakraborty, S. Das, A. K. Nandi, *Prog. Polym. Sci.* **2019**, 88, 189.

The hinge-based bilayer structures consisting of multi-stimuli-responsive hydrogel-based hinges and a temperature-responsive hydrogel matrix can undergo self-folding upon heating and light exposure. The folding angles and kinetics of the bilayer structure are controlled by the geometry of the hinge and different external stimuli, respectively. Furthermore, this single-hydrogel-based bilayer structure demonstrates walking and steering locomotion as autonomous actuators and soft robots.

Programmable Dual-responsive Actuation of Single-hydrogel-based Bilayer Actuators by Photothermal and Skin Layer Effects with Graphene Oxides

Minghao Li, Jinhye Bae*